Analysis of Radiation Pressure and Aerodynamic Forces Acting on Powder Grains in Powder-Based Additive Manufacturing

Sina Haeri[a,*], Soroush Haeri[b], Jack Hanson[a], Saeid Lotfian[c]

[a] *James Weir Fluid Laboratory, Department of Mechanical and Aerospace Engineering, University of Strathclyde, 75 Montrose St, Glasgow, UK, G1 1XQ.*
[b] *Simon Fraser University, Vancouver, British Columbia, Canada*
[c] *Department Of Naval Architecture, Ocean Marine Engineering, University of Strathclyde, Glasgow, UK, G4 0LZ.*

Abstract

Selection of process parameters is an important step in Powder-Based Additive Manufacturing (PBAM) of metals. In order to achieve an optimal parameter set, current literature is mainly focused on the understanding of powder dynamics by analysing the aerodynamic forces. In this letter, however, we show the importance of the laser induced force (radiation pressure) on the powder dynamics. Generalised Lorenz-Mie theory has been employed to accurately estimate the radiation pressure and it is shown that its magnitude is significant in comparison to various aerodynamic forces and the grains' weight, hence, can significantly contribute to denudation and spatter observed in the manufacturing process. Furthermore, the importance of compressibility and rarefaction effects on the magnitude of drag and lift forces that a particle experiences is identified by estimating the Ma and Kn numbers under process conditions, which directly impact the powder dynamics.

Keywords: Additive Manufacturing, Powder Bed, Laser Radiation Pressure, Powder Dynamics

*Corresponding author
Email address: sina.haeri@strath.ac.uk (Sina Haeri)

1. Introduction

The advent of various Powder-Based Additive Manufacturing (PBAM) techniques in the last decade has made it possible to fabricate near net shape parts and components. PBAM components have been utilized by different industrial sectors, such as aerospace, automotive, medical, tools manufacturing, and recently renewable energies to manufacture end parts [1–11].

PBAM is a disruptive technology, which provides a great deal of technological potential and economic advantage [12–14]. Nonetheless, the share of various PBAM processes of the world market for manufacturing is well under 1% [15]. This is mainly attributed to the current technical challenges, which result in manufacturing processes that are hardly repeatable and often can not guarantee to achieve the strict quality standards for critical industrial components without trial builds [16–18]. Overcoming the current challenges is only possible through an in-depth understanding of the underpinning multi-physical processes and their interactions including the powder preparation, laser-powder interaction, heat transfer, and phase changes [19–21]. The currently available mathematical models and in turn the resulting simulation techniques are limited, in that they provide restricted fidelity or only consider one or some of the aforementioned processes in isolation.

Low fidelity pragmatic models have also been devised at specific process conditions [22]. Furthermore, the "continuum" modeling (macro-scale) approaches, which have higher fidelity than the pragmatic models, including the conventional Finite Volume CFD [23, 24] and Finite Element methods [25–27], combined with ad-hoc laser heat source and phase change models have been employed to simulate heat transfer and melt-pool dynamics. Even though these approaches provide insight into the dynamics of the process, their application remains limited owing to the absence of established continuum theories for powder (granular) flow, lack of a clear separation of scales, and abstraction of the multi-physical nature of the process.

High-fidelity particle-scale (micro) simulations are identified as an urgent

technological necessity [28]. Such simulation approaches have been proposed in recent years [29–35] where the Discrete Element Method (DEM) is commonly employed for simulating the effects of powder-bed properties on the manufacturing process [36–44]. The detailed information about the powder-bed may then be used as input to model downstream laser-melting and solidification processes.

To attain a realistic particle-scale simulation, the fundamental forces acting on the grains should be considered. In particular, the impact of the *laser radiation pressure* on the powder dynamics, has not been considered yet. Various undesirable phenomena such as spatter of grains and denudation in metal PBAM processes – such as Selective Laser Melting (SLM) – are attributed to the aerodynamic interactions including recoil pressure, metal vapour jets and the induced inert gas flows [26, 45]. Similar complications arise in other PBAM process such as Laser Metal Deposition (LMD) where only the shielding gas / nozzle flow rates are controlled and no consideration is given to the impact of the laser radiation pressure.

In this communication, we consider the impact of the *laser radiation pressure* on a typical SLM process as demonstrated in Figure 1. First, various lift and drag forces on a particle are calculated. The radiation pressure is then estimated with high precision using the generalised Lorenz-Mie theory (GLMT) and is compared with the aerodynamic forces to asses their relative impact on the powder dynamics.

2. Material and methodologies

For details about optical properties of Inconel grains, methodologies for calculating the aerodynamic forces, estimation of velocity profiles and calculation of radiation pressure using GLMT see the Supplementary material.

3. Results and discussions

Figure 2a shows the drag force experienced by an Inconel particle with $D_p = 30$ μm in the jet region for laser power I varying in the range of 50 W to 200 W.

In this region, the weight of the particle ($W = 1.13 \times 10^{-9}$ N) is several orders of magnitude smaller than the jet drag forces acting on the particle. Therefore, the spatter is mainly attributed to the jet drag forces and the effect of the particle weight on the spatter may be neglected. The negligible impact of grains' weight on their dynamics has also been concluded through high-speed x-ray imaging of the PBAM process [46].

The Mach number varies between Ma = 0.23 and Ma = 0.77 (see the inset of Figure 2a). The drag force scales with Ma^4. Therefore, while for the Mach numbers up to ≈ 0.5, the effects of compressibility remain negligible on the particle's drag force F_D, they rapidly become significant at higher Ma and may cause up to $\%Err = 9$ in the drag force calculations at Ma = 0.77. The rarefaction effects are generally more significant as Kn varies between 0.07 and 0.11, which is in the slip flow regime and enters the transitional flow regime [47] for higher laser powers $I \geq 180$; see Figure 2a where the critical Kn = 0.1 is identified on the inset. The errors in the drag term may be as high as $\%Err = 27$ for Kn = 0.11. It is therefore essential to either apply the appropriate boundary conditions if fully-resolved simulations (see [48–51] for more information about such techniques) of the process are intended or use appropriate corrections for unresolved simulations [52, 53].

Figure 2b shows the radial drag force on the particles for three different particle sizes. The radial drag is strong enough to entrain the particles toward the laser beam from all sides even for largest particle with $D_p = 50$ μm, even though it is 2–3 orders of magnitude weaker than the drag force in the jet region. The Kn number associated with the radial flow region is presented in the inset of Figure 2b, which shows that Kn remains in the slip flow region up to approximately 50 μm away from the beam axis. However, it falls well below the critical value Kn = 0.01 indicating that the rarefaction effects are negligible farther away form the beam axis. Furthermore, due to the presence of a velocity gradient a Saffman force F_S acts on the particles. The induced lift is presented in Figure 2c, which is in an order of magnitude smaller than the radial drag but is still significant compared to the grains' weight. Furthermore, F_S is localised

in the radial direction due to the flow reversals [26], which create regions of low and high velocity gradients.

Perhaps more interesting is the fact that F_S is positive, i.e. downward according to the coordinate system presented in Figure 1. The direction of the lift force F_S is always towards the higher velocity region. While these mechanisms for particle entrainment may appear identical to that of sediment transport in a conventional shear flow set up, which exist in literature [51, 54, 55], they are in-fact distinct because here the shear layer is confined to the vicinity of the laser beam and decays into the quiescent inert atmosphere within a length scale of $\ell \approx 60$ μm. This is comparable to the particle diameter and hence higher velocities are experienced closer to the bed resulting in a downward Saffman lift, which could in-fact stabilise the bed. Nonetheless, the particle Stokes number St, plotted in the inset of Figure 2c, shows the quick response time of the particles in the vicinity of the beam (St $\ll 1$ for up to $r \approx 2D_p$) approaching St $= 1$ for $r \gg D_p$, which indicates nearly inertial particles.

Figure 3 shows the calculated radiation pressure for a particle on the focus plane of the beam. For a circularly polarised beam, $|F_{L,x}|$ in Figure 3a is equivalent to the radiation pressure in a radial direction. In this figure, the value of the $F_{L,x}$ is zero at $x = 0$ as expected and its peak value is positive for $x < 0$ and negative for $x > 0$, which signifies that the particle is pulled towards the beam axis. Furthermore, the curves are symmetric and the peaks occur at approximately $r_0/2$ for all diameters. The smaller particle $D_p \leq 40$ μm does not interact significantly with the beam at large distances $x > r_0$. For the largest tested particle size $D_p = 50$ μm a more complex behaviour is observed: when the centre falls outside of the waist radius (i.e. for $x > 25$ μm), another set of extrema is observed with opposite signs. This indicates that the beam may affect the motion of large particles at distances $x > r_0$ by pushing them away from the beam axis. In comparison to the radial drag forces, the radiation pressure in the radial direction is generally weaker however, it will mainly affect the particles in close proximity of the beam axis at $\approx r_0/2$ whereas the peaks of $F_{D,radial}$ occurs at $\approx 7r_0/5$ and $\approx 12r_0/5$. Nonetheless, $F_{L,x}$ is at least one

order of magnitude greater than W_p for all particle diameters (see the inset of Figure 3a), which confirms the impact of this force on the particle dynamics during the PBAM process.

Figure 3b shows the radiation pressure in the longitudinal direction $F_{L,z}$. The magnitude is approximately two orders of magnitude greater than the particle weight and has the same order of magnitude as F_s but with the peaks occurring at $x = 0$ while the peaks of F_s occur just before and after w_0. Moreover, for $|r_0| < x < |w_0|$, $F_{L,z}$ shows a negative minimum, indicating a lifting effect, interestingly where $F_s \approx 0$. The magnitude of this lifting force is in fact strong enough to levitate the grains and is particularly noticeable for $D_p \geq 40$ μm. This can provide the required instability in the bed leading to entrainment in this region. The axial force $F_{L,z} = 2.6 \times 10^{-7}$ (at $I = 100$ W), is however, two orders of magnitude smaller than the drag force in the vapour jet region $F_{D,jet} = 4.26 \times 10^{-5}$. Nonetheless, we believe that the effects of radiation pressure in the jet region under different conditions can in fact be as significant as the jet drag. For example, Guo et al. [46] estimated a driving pressure in the range of 121 to 931 Pa, with a median of 348 Pa for a more powerful laser ($I = 416$ W) and AlSi10Mg particles with $D_p = 35$ μm (mode value). A direct comparison with Guo et al. [46] is not possible because they do not provide any experimental results for the jet/inert gas velocities. However, a comparison of the the force $F_{D,jet} = 3.3 \times 10^{-7}$, which is resulted from conversion of the driving pressure (348 Pa), with the radiation pressure $F_{L,z} = 3.09 \times 10^{-7}$ calculated at the centre of the beam on the focus plane with $n_r = 1.39 + 9.95$i, $D_p = 35$ μm and the corresponding laser parameters as specified in [46], confirms the significance of the effects of the radiation pressure in the jet region.

The longitudinal and radial radiation pressure for a grain moving along the axis of the beam is shown in Figure 4. The top and bottom panels show $F_{L,x}$ and $F_{L,z}$ for a particle 30 and 5 μm away from the axis. The radiation pressure forces remain notable at long distances of at least $200D_p$ both in the longitudinal and radial directions whereas the $F_{D,jet}$ decays exponentially along the axis of the beam [26]. For a particle at $x_0 = 5$ μm, $F_{L,x}$ remains greater then the

particle weight up to $z \approx 5$ mm for $D_p = 20$ μm and $z \approx 2.5$ for $D_p = 50$ μm (Figure 4 bottom left panel). The magnitude of this force remains negative indicating that the beam will attract the particles toward the axis. Figure 4 bottom right panel shows the longitudinal force which is about two orders of magnitude stronger than the particle weight in the near field region.

The longitudinal radiation pressure acts at much longer distances and remains significant up to $z = 1$ cm (10^4 μm) where the vapour jet and inert gas circulating flows have decayed, and hence, irrelevant. The laser radius changes along its path as $r(z) = r_0(1 + (z/z_R)^2)^{1/2}$, where z_R is the Rayleigh range given by $z_R = \pi r_0^2 n_{env}/\lambda$. The Rayleigh range for the laser under consideration is $z_R \approx 1.9$ mm (assuming $n_{env} = 1$) and hence the slow decay of radiation pressure is expected. Moreover, the laser used in an actual SLM device may have a larger radius of $r_0 = 100$ μm or more compared to the laser experimental rig used in Bidare et al. [26], and hence the action range of the longitudinal force is probably even longer in an actual SLM device.

The top panels in Figure 4 shows the results of the same calculation for a particle moving off-axis at $x_0 = 30$ μm, i.e. the particle centre is initially outside the beam radius r_0. Firstly, note that the force is significant for all particle sizes in both radial and longitudinal directions. For particles with $D_p \leq 40$ μm, the force remains attractive (towards the axis) for all z, but interestingly, the maximum attractive force is experienced at $z \approx 1$ mm. This is due to the fact that at larger distances the particle geometric cross section is initially outside the beam radius and gradually fully enters the beam (remembering that $r = f(z)$) and interacts more with the beam before it feels the decay in the intensity due to the beam divergence. For the largest particle size $D_p = 50$ μm, the behaviour is more complex and the particle initially is repelled form the axis for distances of up to $z = 800$ μm and then attracted towards the beam axis with a maximum attractive force experienced at around $z = 2$ mm. The longitudinal force $F_{L,z}$, similarly, shows a maximum at $z = 3$ mm above the laser waist. $F_{L,z}$ decays very slowly and can impact particle dynamics at distances as far as a few centimetres away from the waist. It is worth mentioning that the laser

may not be focused exactly on the bed and the waist may fall above the bed in practice. However, Figure 4 only presents the results above the beam waist. It should be emphasised that these forces are *not* symmetric around the waist (i.e. z_0 axis) due to the change in the curvature of the wave front at the waist and hence one cannot simply extrapolate them.

4. Conclusions

In this letter, we highlighted the significance of the radiation pressure for the analysis of powder dynamics in the SLM process which had not yet been considered. Following conclusions are drawn based on the comparison of calculated radiation pressure (using generalised Lorenz-Mie theory) and the estimated aerodynamics forces

In the circulation region of the inert gases, the radiation pressure is as significant (same order of magnitude) as the aerodynamic forces. Therefore, to analyse experimental results or for accurate particle-based simulations, their effects should be considered concurrently. The current calculations show that in the vapour jet region, the drag force dominates the radiation pressure. However, it is also shown that under different conditions or for other materials both forces have similar magnitudes. Moreover, contrary to the aerodynamics forces, which are generally localised in the vicinity of the melt pool, the radiation pressure can impact the grains' trajectories at distances of up to 1 cm (and more).

It is also demonstrated that to accurately predict/analyse the powder dynamics, the compressibility and rarefaction effects are important and should be considered in simulations or experimental analysis. The particle asphericity affects the results, however, for most PBAM processes, highly spherical particles are used. Thus, the conclusions are relevant to the actual process. Furthermore, for typical particle roundedness and sphericity values the order of magnitude of various forces will remain the same and current conclusions are still valid.

The axis of the laser beam is assumed to be normal to the powder bed here, whereas in practice, it can be applied at an angle. Therefore, the longitudinal

and normal forces should be transformed to the laboratory coordinate system resulting in a more complex interaction depending on the incidence angle.

In this letter, only a single grain is considered. It is not possible to analytically consider the net effect of these forces on a population of particles. However, the single particle calculations here, demonstrate the need for further investigations of the impact of radiation pressure on the SLM and other metal PBAM processes (e.g. LMD) through particle-based simulations, such as Discrete Element Method (DEM) and systematic experiments. In such a particle-based simulation framework, while the laser-powder interaction may be modeled using GLMT-DEM coupling, the inert gas/metal vapour jet interactions may be modeled through fully resolved or unresolved techniques depending on the required fidelity.

Acknowledgements

The authors gratefully acknowledge the support of EPSRC (Engineering and Physical Sciences Research Council) for the present work under EP/T009128/1 and EP/P007805/1. The authors also wish to acknowledge the funding received from Advanced Forming Research Centre (AFRC) under project AFRC-CATP-1543-R2I via Route to Impact programme.

References

[1] D. D. Gu, W. Meiners, K. Wissenbach, R. Poprawe, International materials reviews 57 (2012) 133–164.

[2] N. Guo, M. C. Leu, Frontiers of Mechanical Engineering 8 (2013) 215–243.

[3] W. E. Frazier, Journal of Materials Engineering and Performance 23 (2014) 1917–1928.

[4] G. Tapia, A. Elwany, Journal of Manufacturing Science and Engineering 136 (2014) 060801.

[5] W. E. King, A. T. Anderson, R. M. Ferencz, N. E. Hodge, C. Kamath, S. A. Khairallah, A. M. Rubenchik, Applied Physics Reviews 2 (2015) 041304.

[6] T. D. Ngo, A. Kashani, G. Imbalzano, K. T. Nguyen, D. Hui, Composites Part B: Engineering 143 (2018) 172 – 196.

[7] H. Fayazfar, M. Salarian, A. Rogalsky, D. Sarker, P. Russo, V. Paserin, E. Toyserkani, Materials & Design 144 (2018) 98 – 128.

[8] C. Culmone, G. Smit, P. Breedveld, Additive Manufacturing 27 (2019) 461 – 473.

[9] A. Adeyemi, E. T. Akinlabi, R. M. Mahamood, Materials Today: Proceedings 5 (2018) 18510 – 18517.

[10] F. Liravi, E. Toyserkani, Additive Manufacturing 24 (2018) 232 – 242.

[11] S. Lotfian, G. Rolink, A. Weisheit, M. Palm, MRS Advances 2 (2017) 1393–1398.

[12] M. Markl, C. Korner, Annual Review of Materials Research 46 (2016) 93–123.

[13] R. Hague, P. Reeves, S. Jones, Mapping UK Research and Innovation in Additive manufacturing, Technical Report, Innovate UK, 2016.

[14] S. on Advanced Manufacturing Committee on Technology, Strategy for American Leadership in Advanced Manufacturing, Technical Report, National Science & Technology Council, 2018.

[15] U. A. M. S. Group, Additive Manufacturing UK: National Strategy 2018 - 25, Technical Report, AM UK, 2018.

[16] B. Mueller, Assembly Automation 32 (2012).

[17] A. S. T. M. C. F. on Additive Manufacturing Technologies, A. S. T. M. C. F. on Additive Manufacturing Technologies. Subcommittee F42. 91 on

Terminology, Standard terminology for additive manufacturing technologies, ASTM International, 2012.

[18] D. L. Bourell, D. W. Rosen, M. C. Leu, 3D Printing and Additive Manufacturing 1 (2014) 6–9.

[19] M. Mani, K. W. Lyons, S. K. Gupta, Journal of research of the National Institute of Standards and Technology 119 (2014) 419.

[20] I. D. Harris, in: Additive Manufacturing Handbook, CRC Press, 2017, pp. 215–224.

[21] T. Furumoto, M. R. Alkahari, T. Ueda, M. S. A. Aziz, A. Hosokawa, Physics Procedia 39 (2012) 760–766.

[22] A. M. Philo, S. Mehraban, M. Holmes, S. Sillars, C. J. Sutcliffe, J. Sienz, S. G. R. Brown, N. P. Lavery, The International Journal of Advanced Manufacturing Technology 101 (2019) 697–714.

[23] C. Qiu, C. Panwisawas, M. Ward, H. C. Basoalto, J. W. Brooks, M. M. Attallah, Acta Materialia 96 (2015) 72 – 79.

[24] S. Haeri, L. Benedetti, O. Ghita, Powder Technology 363 (2020) 245–255.

[25] W. King, A. T. Anderson, R. M. Ferencz, N. E. Hodge, C. Kamath, S. A. Khairallah, Materials Science and Technology (2014).

[26] P. Bidare, I. Bitharas, R. M. Ward, M. M. Attallah, A. J. Moore, Acta Materialia 142 (2018) 107–120.

[27] Z. Zhang, Y. Huang, A. R. Kasinathan, S. I. Shahabad, U. Ali, Y. Mahmoodkhani, E. Toyserkani, Optics & Laser Technology 109 (2019) 297 – 312.

[28] J. A. Turner, S. S. Babu, C. Blue, Advanced Simulation for Additive Manufacturing: Meeting Challenges Through Collaboration, Technical Report, Oak Ridge National Laboratory, 2015.

[29] T. I. Zohdi, Computational Mechanics 54 (2014) 171–191.

[30] T. I. Zohdi, Mathematics and Mechanics of Solids 19 (2014) 93–113.

[31] J. C. Steuben, A. P. Iliopoulos, J. G. Michopoulos, Computer Methods in Applied Mechanics and Engineering 305 (2016) 537 – 561.

[32] J. M. S. Zielinski, S. Vervoort, H.-W. Mindt, M. Megahed, BHM Berg- und Hüttenmännische Monatshefte 162 (2017) 192–198.

[33] J. Weirather, V. Rozov, M. Wille, P. Schuler, C. Seidel, N. A. Adams, M. F. Zaeh, Computers & Mathematics with Applications 78 (2019) 2377–2394. doi:10.1016/j.camwa.2018.10.020.

[34] M. Francois, A. Sun, W. King, N. Henson, D. Tourret, C. Bronkhorst, N. Carlson, C. Newman, T. Haut, J. Bakosi, J. Gibbs, V. Livescu, S. V. Wiel, A. Clarke, M. Schraad, T. Blacker, H. Lim, T. Rodgers, S. Owen, F. Abdeljawad, J. Madison, A. Anderson, J.-L. Fattebert, R. Ferencz, N. Hodge, S. Khairallah, O. Walton, Current Opinion in Solid State and Materials Science 21 (2017) 198 – 206.

[35] M. Bayat, S. Mohanty, J. H. Hattel, International Journal of Heat and Mass Transfer 139 (2019) 95–114. doi:10.1016/j.ijheatmasstransfer.2019.05.003.

[36] Z. Xiang, M. Yin, Z. Deng, X. Mei, G. Yin, Journal of Manufacturing Science and Engineering 138 (2016) 081002.

[37] E. Parteli, T. Pöschel, Powder Technology 288 (2016) 96–102.

[38] S. Haeri, Y. Wang, O. Ghita, J. Sun, Powder Technology 306 (2017) 45–54.

[39] S. Haeri, Powder Technology 321 (2017) 94–104.

[40] W. Nan, M. Pasha, T. Bonakdar, A. Lopez, U. Zafar, S. Nadimi, M. Ghadiri, Powder Technology 338 (2018) 253 – 262.

[41] W. Li, X. Zhang, F. Liou, The International Journal of Advanced Manufacturing Technology 96 (2018).

[42] Q. Han, H. Gu, R. Setchi, Powder Technology 352 (2019) 91 – 102.

[43] H. Chen, Q. Wei, Y. Zhang, F. Chen, Y. Shi, W. Yan, Acta Materialia (2019).

[44] P. S. Desai, A. Mehta, P. S. M. Dougherty, C. F. Higgs, Powder Technology 342‘ (2019) 441–456.

[45] M. J. Matthews, G. Guss, S. A. Khairallah, A. M. Rubenchik, P. J. Depond, W. E. King, Acta Materialia 114 (2016) 33 – 42.

[46] Q. Guo, C. Zhao, L. I. Escano, Z. Young, L. Xiong, K. Fezzaa, W. Everhart, B. Brown, T. Sun, L. Chen, Acta Materialia 151 (2018) 169–180.

[47] E. Loth, AIAA 46 (2008) 2219–2228.

[48] S. Haeri, J. S. Shrimpton, International Journal of Multiphase Flow 40 (2012) 38–55.

[49] S. Haeri, J. S. Shrimpton, Journal of Computational Physics 237 (2013) 21–45.

[50] S. Haeri, J. Shrimpton, International Journal of Heat and Mass Transfer 59 (2013) 219–229. doi:10.1016/j.ijheatmasstransfer.2012.12.012.

[51] S. Haeri, J. S. Shrimpton, International Journal of Heat and Fluid Flow 50 (2014) 1–15.

[52] S. Haeri, J. Shrimpton, Progress in Energy and Combustion Science 37 (2011) 716–740. doi:10.1016/j.pecs.2011.03.002.

[53] J. S. Shrimpton, S. Haeri, S. Scott, Statistical Treatment of Turbulent Polydisperse Particle Systems, Green Energy and Technology, Springer, 2014.

[54] Y. Ninto, H. M. Garcia, Journal of Fluid Mechanics 326 (1996) 285–319.

[55] D. Liu, Q. Chen, Y. Wang, Computer Methods in Applied Mechanics and Engineering 200 (2011) 1691 – 1707.

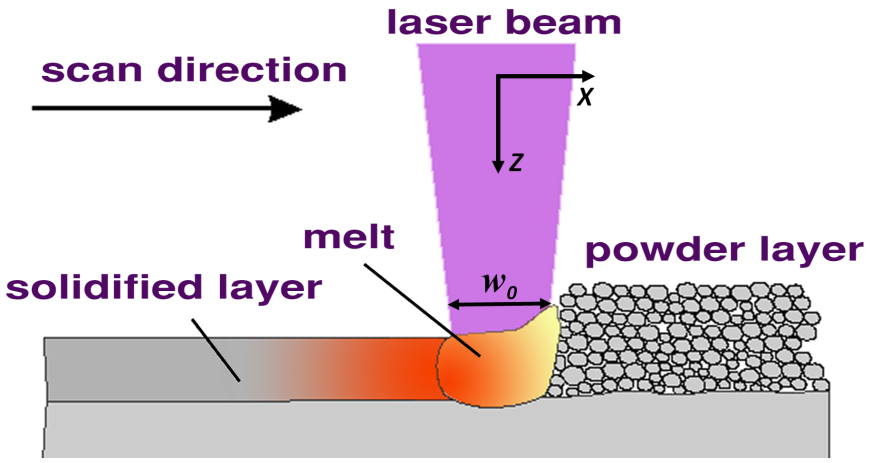

Figure 1: A schematic presentation of the SLM process. A thin layer of powder is spread on a build plate and a thermal energy source is used to selectively fuse the regions of powder bed at desired locations based on a CAD model. After completion of a layer, a repetition of the fabrication process will be accomplished by applying a new layer of powder until a 3D component is fabricated.

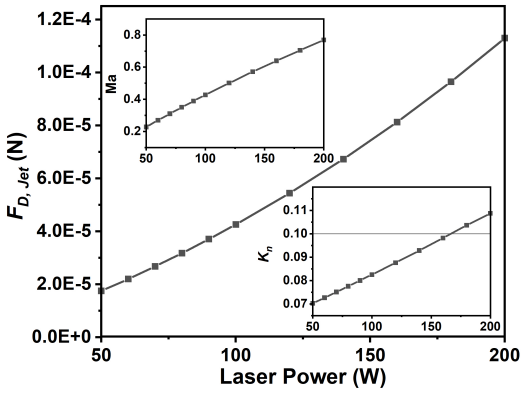

(a)

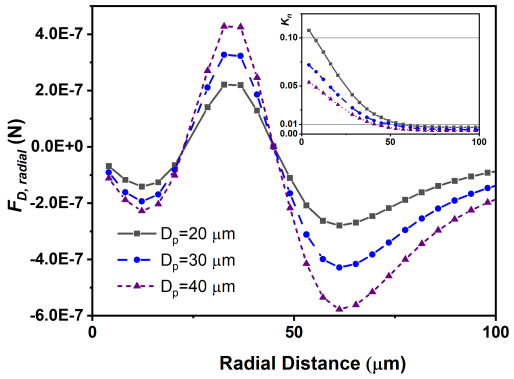

(b)

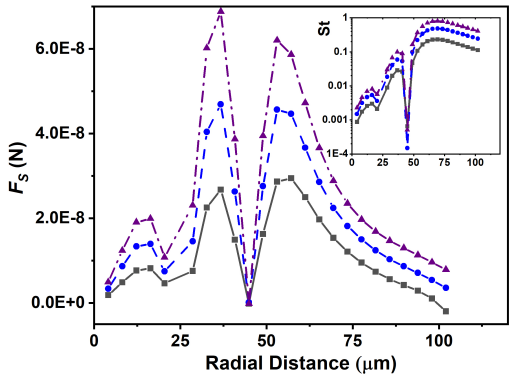

(c)

Figure 2: Estimation of various forces acting on a spherical particle during the SLM process. Figure 2a shows the drag forces on the particle as a function of laser power and the insets show the variation in Kn and Ma in the jet region. Figures 2b and 2c respectively show the drag and Saffman lift forces in the radial flow region (induced by the jet) for a 100 W laser with the Kn and St numbers plotted on the insets.

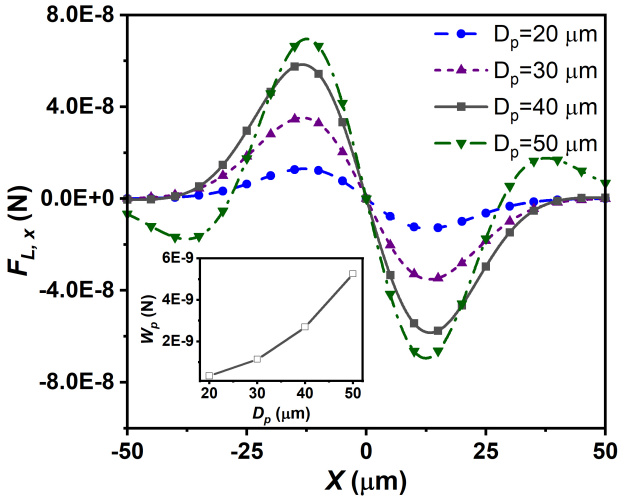

(a)

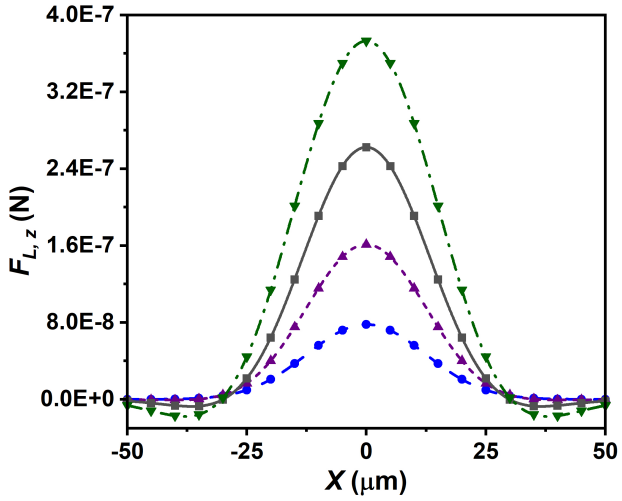

(b)

Figure 3: The estimated radiation pressure on a single powder grain in the focus plane of a Gaussian beam. A laser beam with an intensity of $I = 100$ W, wavelength $\lambda = 1.06$ μm and a waist radius of $r_0 = 25$ μm is assumed. See Figure 1 for the definition of the directions x and z. The inset of Figure 3a shows the particle weights for $D_p = 20 - 50$ μm. The range of the calculations has been limited to $|X| < 50\mu$m since $F_{L,z} \to 0$ as the particle geometric cross section entirely leaves the beam's waist.

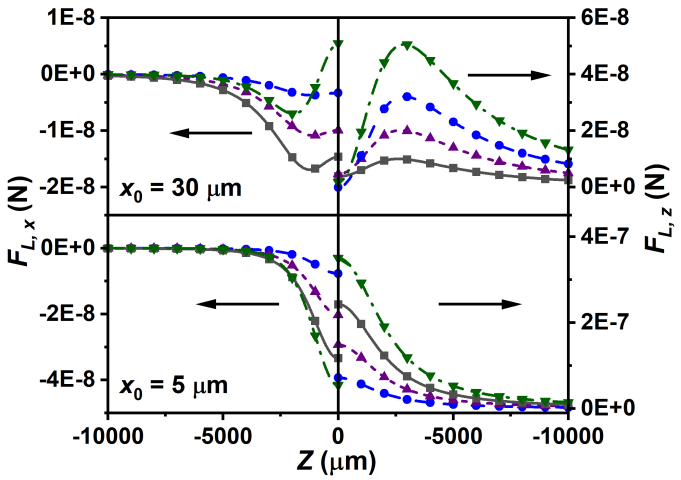

Figure 4: The estimated radiation pressure forces experienced by a powder grain moving off the axis of the beam at two different distances. The laser parameters are specified in the caption of Figure 3. The curves are presented only for the region before the waist at $z = 0$.